Distributions of Soil, Rock, and Grass in the Western Foothills of the Sierra Nevada

John F. Mustard
Department of Geological Sciences
Brown University, Providence RI

Abstract

A linear mixing model is used to model the spectral variability of an AVIRIS scene from the western foothills of the Sierra Nevada. This approach permitted a preliminary estimate of the ground reflectance to be derived. Residual calibration issues that remain are well understood and will be corrected in the future. Five spectral endmembers from the AVIRIS data plus a model shade were used to model the continuum reflectance of each pixel of the AVIRIS image. Three of these endmembers exhibit spatial associations and spectral properties that are best interpreted as different soil types. Composition is clearly a controlling factor on the observed distributions of the different soil types.

I Introduction

Understanding the role of soils as an element in the global climatic web is an important new direction identified as part of NASA's Land Processes investigations. Soils represent the interface between the atmosphere and solid earth and mark a dynamic region for the formation, evolution, and exchange of gases, organic compounds, and mineral constituents. An important step towards determining the global implications of soil processes is developing an inventory of soil types and their spatial distributions. This information also plays a fundamental role in unravelling time dependent evolution of landscapes and climatic influences. It is desirable to identify and map soil types from remote sensing platforms to take advantage of the synoptic perspectives vital to understanding regional to global scale issues. Initial results of an investigation to map the spatial distribution and abundance of surface materials with an emphasis on soil distributions are presented here. In this investigation, AVIRIS data are used, in coordination with laboratory spectral data and analyses, to conduct the majority of the tasks because of the significant advantages of high spectral and spatial resolution data for discriminating subtle differences in soil properties.

II Field Site

The location of this study lies primarily within the Kaweah serpentinite melange in the western foothills of the Sierra Nevada near Fresno CA (Figure 1). The topography is hilly, but smoothly varying with few extensive rock faces or cliffs and a maximum topographic variation of ≈200 meters. The substrate lithology of the region is dominated by the components of a tectonically deformed ophiolite melange in the western half of the site and volcanoclastic sediments and plutonic rocks of the Sierra Nevada in the eastern half. The distribution of primary rock types and general mineral constituents of the melange is well known from extensive field studies conducted by J. Saleeby (Saleeby, 1977; 1978; 1984). Substantial blocks of the coherent ophiolite components generally occupy the higher topographic regions while the intervening regions are composed of the compositionally complex melange. The overall composition of the substrate is mafic to ultramafic and therefore contains abundant magnesium and iron and little potassium, sodium, etc. The extent of the melange can readily be recognized by the distinct lack of trees and uniform cover of soils and grasses. In regions with little or no rock exposure the surface is composed of a mixture of grasses and soil. Although the abundance of grass is quite variable, 100%, or even 50% cover by grass is rare the soils are generally well exposed.

Surface Materials

There are four primary surface materials exposed in the field site: green vegetation, senescent grasses, rock, and soil. Green vegetation will not be treated in any detail since it is restricted primarily to irrigated fields, active water courses, and hills in the northeastern corner of the site.

The lithologic components underlying this region are extraordinarily complex and diverse. Because of the primarily mafic and ultramafic mineralogy, these components are well distinguished by visible to near-infrared reflectance spectra. A selection of reflectance spectra representative of the diversity of the block and matrix lithologies is shown in Figure 2a. These materials are both characterized and distinguished by the strength, position, and shape of the broad ferric and ferrous absorptions between 0.5 and 1.4 μm and the narrow hydroxyl overtone and combination overtones near 1.4 μm and longwards of 1.8 μm. Based on the characteristics of these spectral features it is possible to identify the mineral species (i.e. Burns, 1970; Farmer, 1974; Hunt and Salisbury, 1970), the abundance of minerals (Clark 1987; Mustard and Pieters, 1987a; 1989), and estimate the chemical composition of the minerals (Sunshine, et al, 1990; Mustard, 1990).

Laboratory reflectance spectra of representative vegetation components are shown in Figure 2b. The spectra of the grasses are the most important for this analysis and will be discussed briefly. The spectrum of senescent grass is characterized by a very steep and smooth rise in reflectance between 0.4 and 0.7 μm with cellulose, lignin, and molecular water absorptions longwards of 1.2 μm (Elvidge, 1988). The spectrum of partially decayed grasses differs from senescent grasses primarily in the shape of the spectrum between 0.3 and 1.3 μm where the decay grasses exhibit a distinct slope. The differences in albedo are not considered important since this depends on the albedo of the starting material (i.e. stalks, leaves, seed pods). All components of senescent grasses exhibit broadly similar spectral features but the overall albedo varies with the plant part. Fires are not uncommon in this region and a spectrum of burnt grass is included for comparison to the green and senescent vegetation.

Laboratory reflectance spectra of bulk soil specimens collected from the field site are shown in Figure 2c. Common to all these spectra are the bound water and hydroxyl absorptions near 1.4 and 1.9 μm. Longwards of 2.0 μm are narrow absorptions near 2.2 and 2.3 μm probably due to Al-OH and Mg-OH combination overtones. In the visible to near-infrared wavelength region (0.3 to 1.7 μm) the spectra of these soils are distinguished by iron absorptions. The reddish soil (D) exhibits a strong absorption near 0.5 μm and a weak absorption near 0.9 μm indicating the presence of ferric iron. The two strongly sloped spectra of soils B and C also exhibit weak ferric absorptions. The strong positive slope towards longer wavelengths indicates the probable presence of ferrous iron as well.

III Analysis

Data Reduction and Calibration Estimates

AVIRIS data were acquired over this region on October 2, 1989 under generally clear conditions. Although it was not possible to coordinate field activities for this overflight, field observations, collection of surface samples, and measurement of field reflectance using the PIDAS spectrometer had been accomplished in June and September 1987. There are few time invariant, large spatially and compositionally homogeneous regions of the surface in the AVIRIS window that could be used as calibration targets. However an extensive library of spectra representative of the surface materials in the field site has been developed and therefore the mixing method approach to calibration discussed in detail by Smith et al (1990) and Gillespie et al (1990) was employed as a guide for calibration. The raw AVIRIS data were first corrected to radiance using engineering and calibration files provided by JPL. These corrected data were inspected channel by channel for data quality and image channels with poor quality were discarded. For this analysis only data from the A, B, and C spectrometers were used. A total of 104 channels out of 160 was selected. A subsection of the total image that included agricultural lands was then extracted. An interactive linear mixture analysis was performed on this subset to identify the image endmembers. A small number of image endmembers were selected that best describe the overall spectral properties of the scene. For the initial subset of the total scene 4 image endmembers plus shade were required to accurately model the scene radiance.

The 4 image endmembers were then compared to the spectral library developed for this site using the linear gain, offset, and fractional abundance relationships given by Smith et al (1990) and Gillespie et al (1990). The purpose of this analysis was to derive a set of calibration coefficients to

correct for the additive and multiplicative effects of instrument and atmosphere and thereby convert the AVIRIS radiance to an estimate of surface reflectance. Convergence to an acceptable solution was hindered by the low spectral contrast between the image endmembers and the lack of relevant vegetation spectra in the spectral library used. Nevertheless inspection of the gain and offset factors indicated little variation among the solutions for the offset term. Since the additive terms are more critical than the multiplicative terms for mathematical analyses of spectra, an average of the offset terms from several solutions was subtracted from the AVIRIS radiance. To convert to reflectance a region of apparent homogeneous grass cover was used as a relative reflectance calibration standard (Mustard and Pieters, 1987b). A plot of the multiplicative and additive terms used to convert the AVIRIS radiance to approximate reflectance is shown in Figure 3. Note that the additive term shows an exponential decrease with increasing wavelength typically of atmospheric scattering. There are still lingering calibration difficulties at this stage and refinements of the calibration are continuing.

Spatial Distributions

In the initial linear mixing analysis of the raw data, a subset of the total AVIRIS scene was used to expedite the analysis and interpretation of results. Using the data corrected for estimates of the additive and multiplicative calibration factors (calibrated data) this analysis was expanded to encompass the entire image. In addition to the four image endmembers identified during data reduction, a fifth image endmember was required to achieve an acceptable solution. This is the minimum number of endmembers that could be selected to model the image. The spatial distribution and abundance of the 5 image endmembers plus a model shade of 0.01% reflectance to account for illumination effects (Adams et al, 1986; Smith et al, 1990) are shown in Figure 4 along with an image of the total rms error of the fit of the image endmembers to each spectrum in the image. All calculations were carried out at the full dynamic range of the AVIRIS data. The average rms error for the entire image is less than 3% reflectance. Inspection of the rms error image shows a high quality fit with only a few regions of high error. However inspection of error as a function of wavelength or band residual images shows a few wavelength regions (0.7-0.8 μm, 1.5-1.65 μm) where the error is correlated with illumination indicating errors in the removal of additive terms in the calibration.

Nevertheless, the fraction images reveal many interesting relationships amongst the surface components. Note that the fraction images are largely uncorrelated with illumination (compare to the complimented shade image). This indicates that the only the fractional contributions from the actual spectral endmembers are being identified and not effects of illumination. The elements of green vegetation are extremely well modelled and partitioned into the vegetation fraction image which illustrates that vegetation is localized in irrigated fields and along water courses. The grass endmember is highly correlated with albedo (though not illumination) but the spatial patterns agree with general field observations. The other three images are thought to represent the distributions of different soil units. Soil1 exhibits a broad diffuse pattern and is concentrated in the western and south western portion of the image. In this region the substrate is dominated by lithologies of the ophiolitic melange and suggests that the spectral properties of this soil unit are strongly influenced by this substrate material. High values in the Soil2 fraction image exhibit a strong association with valley floors in the western portion of the image and also in a spatially coherent arcuate zone extending towards the southeast of the image. This arcuate zone correlates with a fault block of ophiolitic material which also suggests an physical association between this soil unit and substrate composition. However the association of this same soil unit with restricted valley bottoms implies alternative explanations. Finally distributions of Soil3 are strongly concentrated in the eastern portion of the image over substrates dominated by plutonic and volcanoclastic rocks. This again implies a strong association between substrate and soil compositions.

As discussed in detail by Gillespie et al (1990) and Roberts et al (1990), linear mixture analysis primarily models overall spectral continuum. Surface materials that exhibit small amplitude and narrow absorptions not contained in the spectra of the model endmembers may be identified through analysis of band residual images. Also materials that demonstrate nonlinear mixing systematics may be identified on the basis of band residual images. By using the wavelength

dependent character of band residual errors it is possible to identify unmodelled compositional elements of the surface and their spatial distributions. Analysis of band residual images for the Kaweah field site to identify spectral elements of the surface not accounted for with the linear mixture model is continuing. The foci of this analysis are the Fe^{3+} and Fe^{2+} absorptions between 0.5 and 1.4 μm specifically to identify any exposed rock outcrops which are expected to have significantly stronger iron absorptions and to detect subtleties in the iron mineralogy of the soils. Although there are several intriguing possible relationships evident the analyses to date, a thorough band residual analysis must wait for the resolution of the lingering calibration issues.

Endmember Spectral Properties

AVIRIS approximate reflectance spectra of the 5 image endmembers used to compute the distribution and abundance of surface components are shown in Figure 5. These spectra are averages of about 20 spectra each. The grass spectrum exhibits the characteristic steep rise in reflectance and smoothly varying spectrum discussed above. The green vegetation spectrum exhibits classic features of green vegetation such as the 0.55 μm reflectance peak and the sharp edge of the chlorophyll absorption near 0.7 μm. The soil spectra are distinguished primarily by the shape of the spectrum between 0.5 and 1.3 μm and the character of the spectra between 1.5 and 1.7 μm. Clearly some of these "soil" endmembers contain senescent vegetation which is indicated by a reflectance maximum near 1.65 μm. This is likely partially decayed grasses with spectral properties discussed above. The other soil components which do not exhibit the 1.65 μm reflectance peak nor a drop in reflectance between 1.35 and 1.5 μm are likely to be primarily composed of soil. Note that the soil spectra between 0.7 and 1.0 μm are clearly lower in reflectance that the continuum on either side of this section. This is an artifact of the calibration and is seen to be correlated with a similar feature in the the plot of the offset terms in Figure 3. The correlation of this spectral segment with the red edge and near infrared plateau of the green vegetation spectrum implies that the green vegetation spectra in our library are inappropriate to model the vegetation components in this scene.

IV Conclusion

General distributions and abundances of the major surface components in the foothills of the Sierra Nevada were determined using a linear mixing model. Three of the endmembers are apparently related to different soil types and the distributions of these soils have strong associations with substrate lithology. This implies a strong link between the soil spectral properties and substrate lithology. Only the broad, continuum spectral properties have been modelled in this analysis and only with image endmembers. A refined calibration will be obtained and a spectral library used to derive more accurate analysis of surface components. Also the band residual images will be investigated in detail following the final calibration to provide additional constraints on spectral variability and soil compositions. Nevertheless, this preliminary analysis has clearly demonstrated that subtle soil spectral properties are distinguished using quantitative modelling approaches of imaging spectrometer data and that these soil properties can be mapped.

References

Adams, J. B., M. O. Smith, and P. E. Johnson, Spectral mixture modeling: A new analysis of rock and soil types at Viking Lander 1, J. Geophys. Res., 91, 8113-8125, 1986.

Burns, R. G., Mineralogical Application to Crystal Field Theory. Cambridge University Press, London. 224 pp. 1970.

Clark, R. N., Deconvolution of reflectance spectra of mineral mixtures into component abundance and grain size (abstract), Trans. of Am. Geophys. Union, 68, 464, 1987.

Elvidge, C. D., Vegetation reflectance features in AVIRIS data, Int'l Symposium Rem. Sens. Envir. Sixth Thematic Conference on Remote Sensing for Exploration Geology, 169-182, 1988.

Farmer, V. C. ed., The Infrared Spectra of Minerals, The Mineralogical Society, London, pp. 539, 1974.

Gillespie. A. R., M. O. Smith, J. B. Adams, S. C. Willis, A. F. Fischer III, and D. E. Sabol, Interpretation of residual images: Spectral mixture analysis of AVIRIS images, Owens Valley, California, in Proc. of the Second Airborne Visible/Infrared Imaging Spectrometer (AVIRIS) Workshop (R. O. Green, ed.) JPL publication 90-54, 243-270, 1990.

Hunt, G. R., and J. W. Salisbury, Visible and near-infrared spectra of minerals and rocks: I Silicate minerals. Mod. Geol., 1, 283-300, 1970.

Mustard, J. F., and Pieters C. M., Quantitative abundance estimates from bidirectional reflectance measurements. Proc. Lunar Planet. Sci. Conf. 17th, Part 2, in J. Geophys. Res., 92, E617-E626, 1987a.

Mustard, J. F., and Pieters C. M., Abundance and distribution of ultramafic microbreccia in Moses Rock Dike: Quantitative application of mapping spectrometer data. J. Geophys. Res., 92, 10376-10390, 1987b.

Mustard, J. F., and C. M. Pieters, Photometric phase functions of common geologic minerals and applications to quantitative analysis of mineral mixture reflectance spectra, J. Geophys. Res., 94, 13619-13634, 1989.

Mustard, J. F., Methods of quantitative analysis of reflectance spectra and application to imaging spectrometer data, Ph.D. Thesis, Brown University, Providence RI, USA, pp. 231 1990.

Roberts, D. A., M. O. Smith, J. B. Adams, D. E. Sabol, A. R. Gillespie, and S. C. Willis, Isolating woody plant material and senescent vegetation from green vegetation in AVIRIS data, in Proc. Second Airborne Visible/ Infrared Imaging Spectrometer (AVIRIS) Workshop (R. O. Green, ed.) JPL publication 90-54, 42-57, 1990

Saleeby, J. B., Fracture zone tectonics, continental margin fragmentation, and emplacement of the Kings-Kaweah ophiolite belt, southwestern Sierra Nevada, California, in R. G. Coleman and W. P. Irwin (eds.) North American Ophiolites, Oregon Dept. Geol. Min. Ind. Bull., v 91, p 141-160, 1977

Saleeby, J. B., Kaweah serpentinite melange, southwest Sierra Nevada foothills, California, Geol. Soc. Am. Bull., v 90, p 24-46, 1978.

Saleeby, J. B., Tectonic significance of serpentinite mobility and ophiolite melange, in L. A. Raymond (ed) Melanges; Their nature, origin, and significance, Geol. Soc. Am. Special Paper 198, 153-168, 1984.

Smith, M. O, Ustin, S. L., Adams, J. B., and A. R. Gillespie, Vegetation in deserts: I A regional measure of abundance from multispectral images, Remote Sensing of Environment, 31, 1-26, 1990.

Sunshine, J. M., C. M. Pieters, and S. F. Pratt, Deconvolution of mineral absorption bands: An improved approach, J. Geophys. Res, 95, 6955-6966, 1990.

Acknowledgements: Support from NASA grant NAGW-1118 is gratefully acknowledged. Many thanks to Rob Green for assistance in collecting field spectra with the PIDAS instrument, C. Pieters for thoughtful discussions, and to J. Adams, M. Smith, and S. Willis at the University of Washington for an introduction to the linear mixing approach to data reduction.

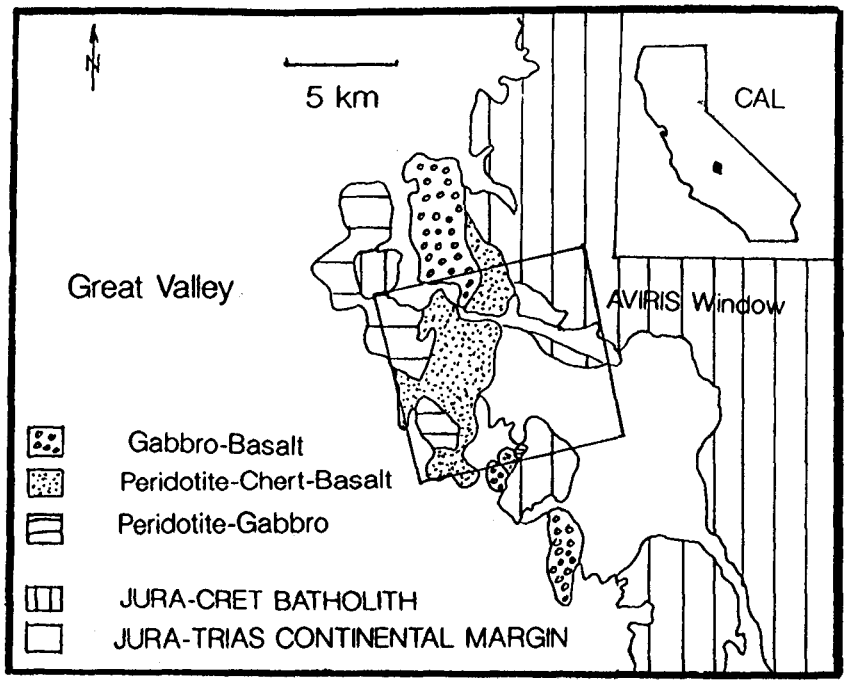

Figure 1. Generalized bedrock geology map of the region of the western foothills of the Sierra Nevada investigated (after Saleeby, 1979). The AVIRIS window used in this investigation is outlined.

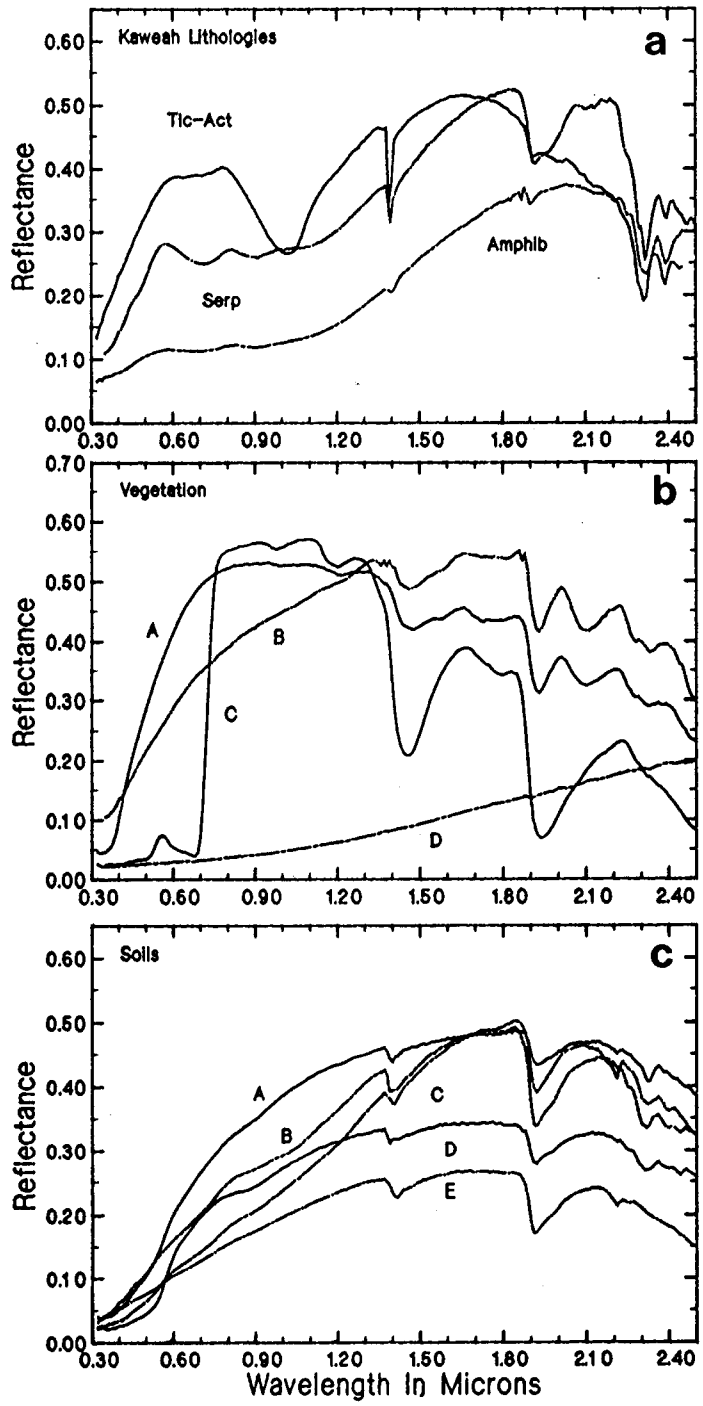

Figure 2. Representative laboratory reflectance spectra of the major lithologic, vegetative, and soil types from the field sites. All spectra were measure in RELAB at Brown University. For the vegetation spectra, A is senescent grass, B is partially decayed senescent grass, C is green vegetation (maple leaf) and D is burnt grass. For the soil spectra note the presence of a distinct 2.3 μm hydroxyl absorption in most of the soils and 2.2. μm absorption in some. Also note the ferric and ferrous absorptions in the strongly oxidized soil (D) and the steep spectral slopes in the spectra B and C relative to the more concave continua of spectra A, D, and E.

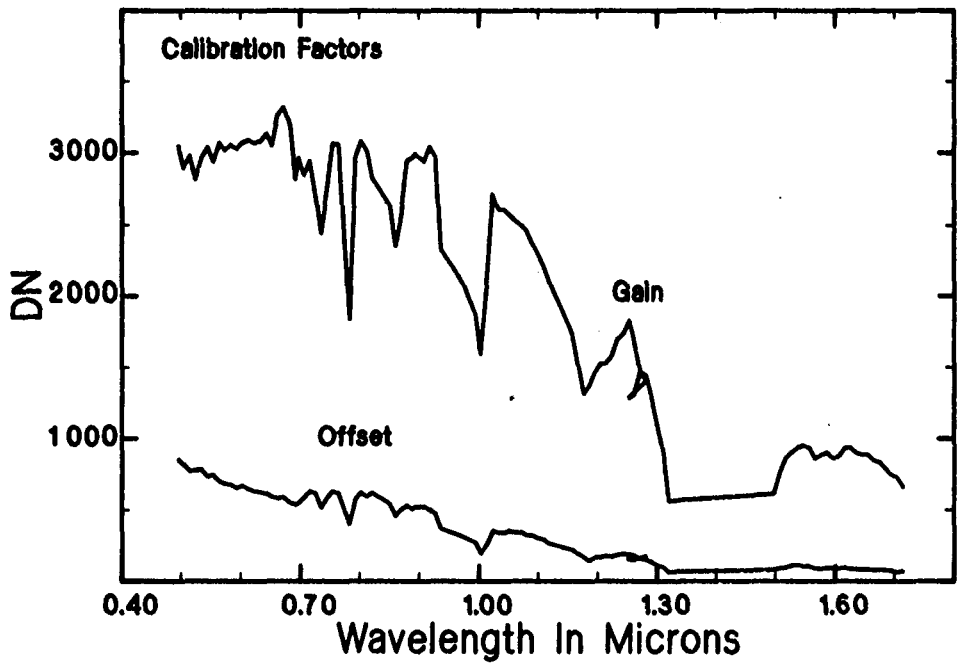

Figure 3. Gain and offset terms used to calibrate the AVIRIS radiance data to reflectance. Offset terms were determined using a linear mixing approach (i.e. Gillespie et al, 1990) and gain values were determined by a relative reflectance method (Mustard and Pieters, 1987b).

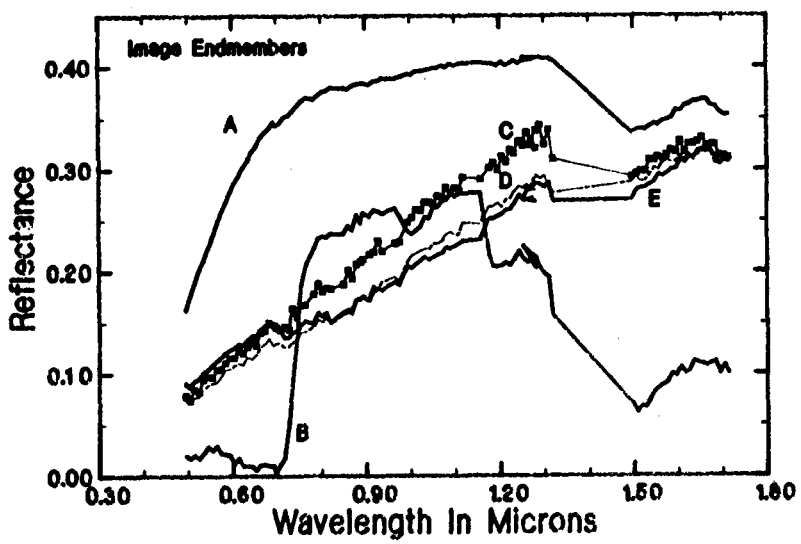

Figure 5. AVIRIS reflectance spectra of the image endmembers used to calculate the surface abundances shown in Figure 4. A is the GRASS endmember, B is the VEGETATION endmember, C is SOIL2, D is SOIL1 and E is SOIL3. There are small calibration errors evident between 0.7 and 1.0 μm that are currently being corrected. The soil endmembers are distinguished primarily by differences in slope and the strength of the senescent vegetation absorptions between 1.5 and 1.7 μm.

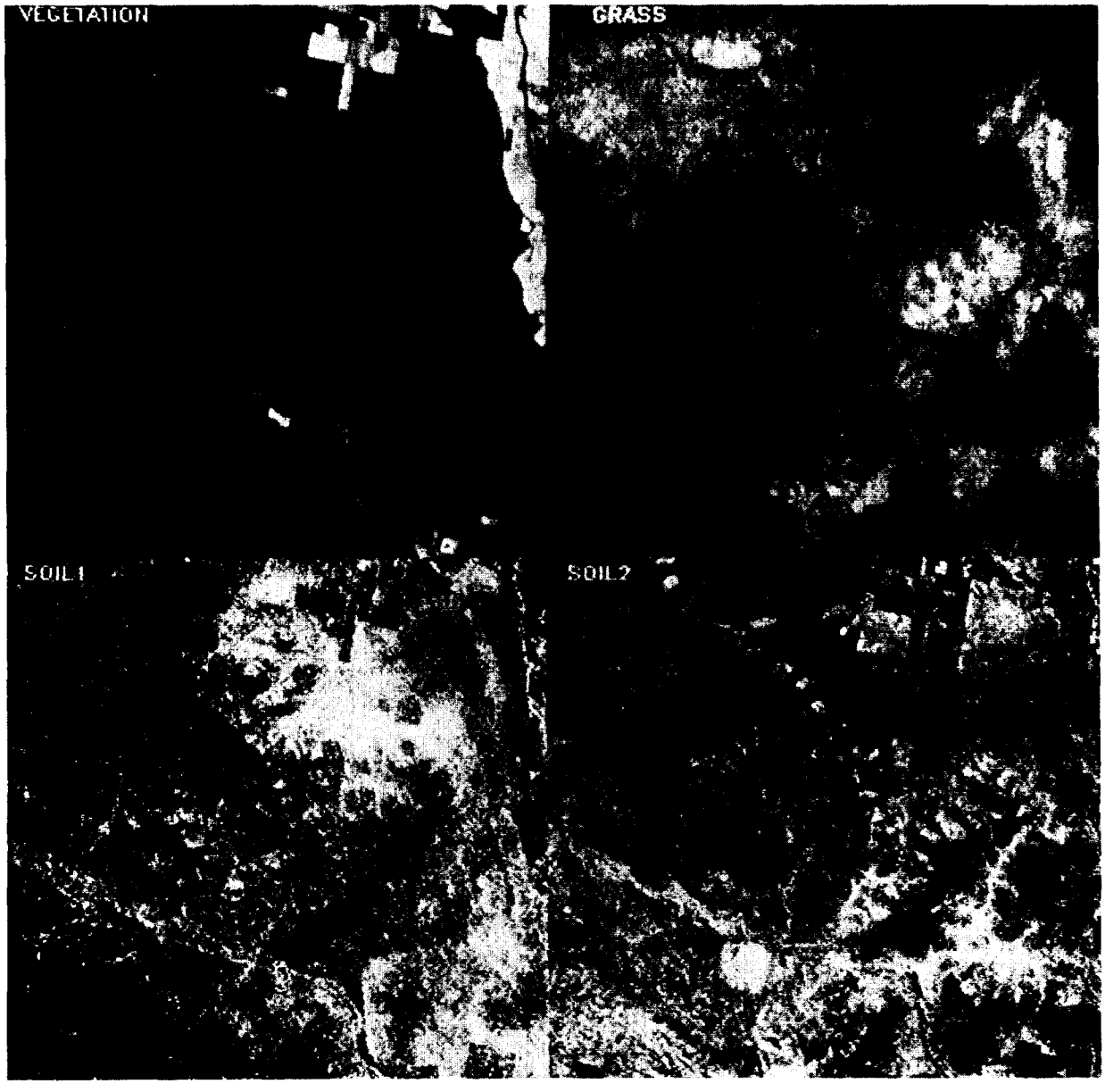

Figure 4. These images present the solution to the linear mixing equation applied to the AVIRIS data using image endmembers. Each image shows the spatial distribution and abundance of an image endmember where bright values represent higher abundance. The label for each abundance image in the upper left corner gives an interpretation to the most abundance surface component in the endmember. Discussion of the distributions is given in the text. The "SHADE" abundance image has been complimented. The "VARIANCE" image shows the total RMS error of the fit of the image endmembers to each pixel and for this solution the average RMS error is 75 DN or about 2-3% reflectance. Spectra of the image endmembers used in the calculations are shown in Figure 5. North is towards the bottom in all these images and the ground coverage of the AVIRIS data is shown in Figure 1.

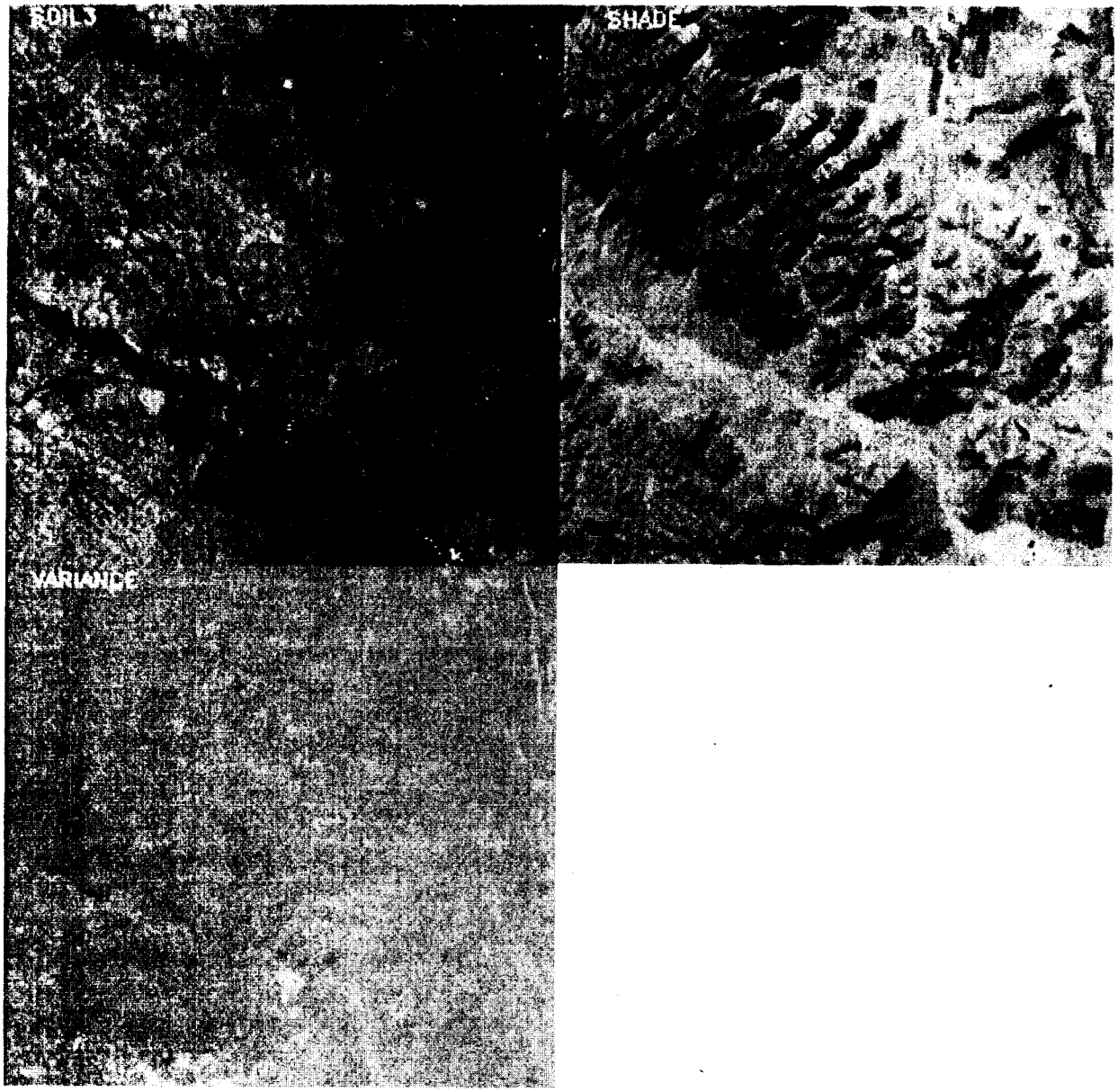

Figure 4 (cont'd)